Chemical Science

rsc.li/chemical-science

EDGE ARTICLE
Tosaporn Sattasathuchana, Breno R. L. Galvão, Rui Sun,
Ralf I. Kaiser *et al.*
Gas-phase synthesis of the bicyclic silicon tricarbide
molecule (c-SiC$_3$) as a precursor to silicon carbide
nanoparticles in space

**ROYAL SOCIETY
OF CHEMISTRY**

EDGE ARTICLE

Check for updates

Gas-phase synthesis of the bicyclic silicon tricarbide molecule (c-SiC₃) as a precursor to silicon carbide nanoparticles in space

Shane J. Goettl, [a] Kazuumi Fujioka,[a] Márcio O. Alves,[b] Mateus X. Silva, [†b]
Zhenghai Yang,[a] Surajit Metya, [a] Iakov A. Medvedkov, [a]
Tosaporn Sattasathuchana,*[a] Breno R. L. Galvão, *[b] Rui Sun *[a]
and Ralf I. Kaiser *[a]

Silicon–carbon bond couplings represent a fundamental foundation for bottom-up molecular mass growth processes of silicon carbide grains in extraterrestrial environments. Yet, the elementary reaction mechanisms affording the gas-phase preparation of simple silicon- and carbon-containing molecules, which act as central molecular building blocks of silicon carbide grains, remain largely unexplored. Herein, we reveal the barrierless gas-phase preparation of the bicyclic silicon tricarbide molecule (c-SiC₃, X^1A_1) and its linear isomer (l-SiC₃, $X^3\Sigma^-$) as prototype silicon carbide grain precursors *via* the bimolecular reaction between tricarbon (C_3, $X^1\Sigma_g^+$) and silylidyne (SiH, $X^2\Pi$) under single-collision conditions. With the detection of c-SiC₃ and l-SiC₃ in the circumstellar envelope of the carbon star IRC+10216, the title reaction offers an entrance point for the exotic silicon chemistry in deep space thus bringing us closer to an understanding of how silicon and carbon chemistries can be coupled in our galaxy.

Introduction

Ever since the detection of the cyclic silicon dicarbide molecule (SiC_2, X^1A_1) in the circumstellar envelope of the asymptotic giant branch (AGB) carbon star IRC+10216 more than 60 years ago,[1] silicon–carbon clusters have emerged as fundamental molecular building blocks of silicon carbide nanoparticles in deep space as identified *via* their 11.3 μm (885 cm^{-1}) emission line (Fig. 1).[2] These silicon–carbon clusters are characterized through unique chemical bonding schemes, which are distinct from their iso-valent carbon–carbon counterparts. For instance, tricarbon (C_3, **1**, $X^1\Sigma_g^+$) is linear and has a singlet ground state, which is favored by 84 kJ mol^{-1} compared to the equilateral triangle structure in its A_2' triplet ground state (**2**).[3] However, in case of silicon dicarbide (SiC_2), the cyclic isomer (**3**) is advantaged energetically by 220 kJ mol^{-1} compared to the linear isomer (**4**) (Fig. 2a).[4] In the tetratomic system (Fig. 2b), tetracarbon (C_4) is most stable in its linear geometry and holds a $^3\Sigma_g^-$ ground state (**5**) with a low-lying, bicyclic rhombic isomer only 9 kJ mol^{-1} higher in energy (**6**).[5] Silicon tricarbide (SiC_3), on the other hand, features exotic C_{2v} symmetric bicyclic isomers with either bisecting carbon–

carbon (**7**) or silicon–carbon (**8**) bonds, which are favorable by 34 and 9 kJ mol^{-1} compared to the linear triplet isomer (**9**).

This stability of cyclic *versus* acyclic silicon carbides can be in part rationalized through the concept of aromaticity. Natural bond order (NBO) analysis of cyclic silicon dicarbide (**3**) predicts an optimal Lewis structure with delocalization of two π electrons between the silicon and carbon atoms.[6] However, c-SiC₂ exhibits a significant ionic character between the silicon atom and the dicarbon moiety[7] thus categorizing **3** as polytopic[8] with the dicarbon group undergoing a hindered rotation (pinwheel motion).[9–11] The classification of silicon tricarbide (**7**) depicts a delocalization of two π electrons over one or both rings,[12,13] while the higher energy linear isomer (**9**) features characteristic cumulenic bonding.[14] The c-SiC₃ structure which contains a silicon–carbon bisection (**8**) represents a fascinating benchmark with π electron delocalization only along the C₃ moiety, which does not overlap with the silicon π orbitals or lone pair.[15] Overall, the introduction of a single silicon atom into a carbon framework results in fundamental changes in the chemical bonding, aromaticity, molecular structure ((bi)cyclic *versus* linear), and electronic properties (triplet *versus* singlet), which are not predictable by Langmuir's concept of isovalency.[16]

However, despite the critical importance of silicon carbides in astrochemistry,[17–20] material sciences (catalysis,[21] nano-structures,[22,23] semiconductors[24]), and physical (organic) chemistry from the viewpoint of chemical bonding and molecular structure, the controlled gas-phase preparation of silicon carbides has been scarce. Previous work involved laser ablation of silicon carbides[25–28]

[a] Department of Chemistry, University of Hawai'i at Mānoa, Honolulu, HI 96822, USA. E-mail: ralfk@hawaii.edu; ruisun@hawaii.edu; tsatta@hawaii.edu

[b] Centro Federal de Educação Tecnológica de Minas Gerais, Belo Horizonte 30421-169, Brazil. E-mail: brenogalvao@gmail.com

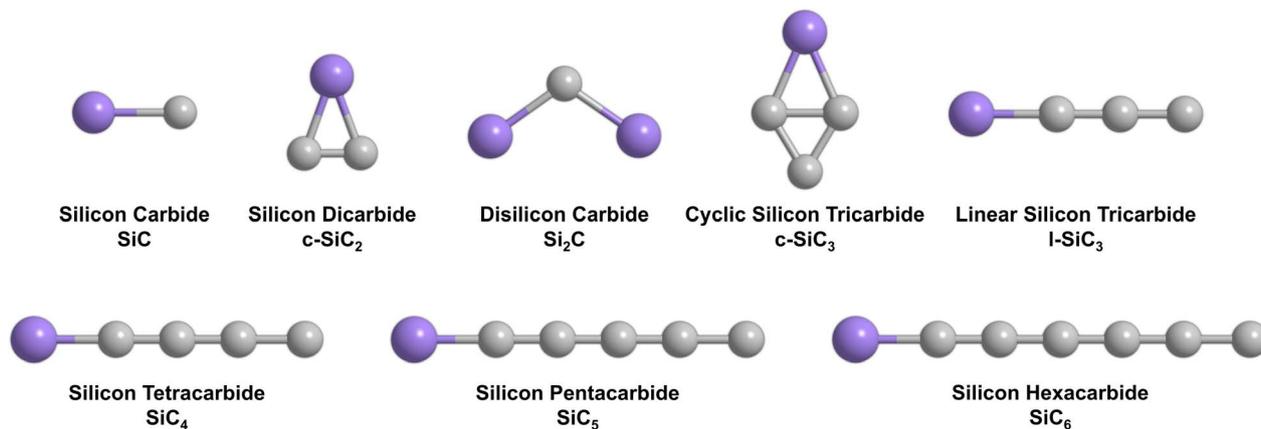† Present address: Departamento de Química, Universidade Federal de Ouro Preto, Minas Gerais 35402-136, Brazil.

Fig. 1 Silicon- and carbon-containing hydrogen-deficient molecules which have been identified in interstellar and circumstellar environments. Silicon and carbon are depicted as purple and gray, respectively.
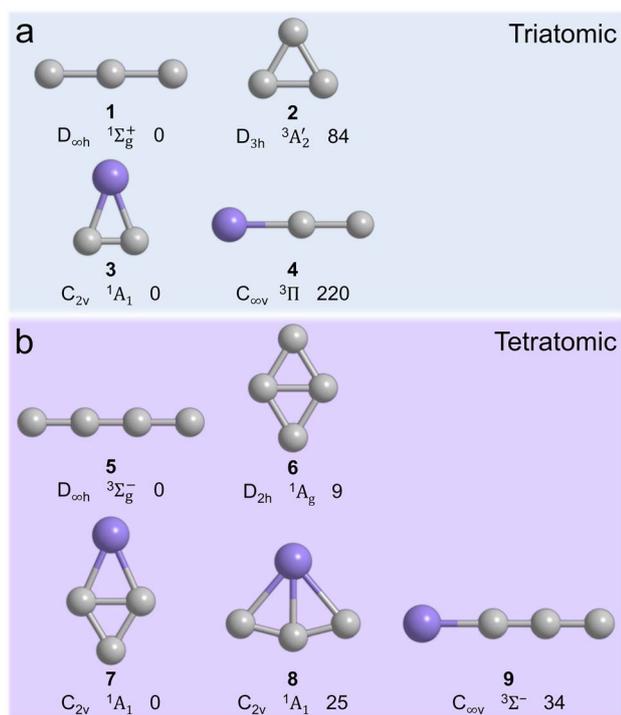

Fig. 2 Comparison of the structures of the most stable triatomic (a) and tetratomic (b) molecules containing only carbon *versus* those in which one carbon atom is substituted by atomic silicon. Point groups, electronic states, and relative energies (kJ mol^{-1}) are also provided from left to right for each structure. Silicon atoms are purple and carbon atoms are gray.

along with electric discharge of mixtures of silicon- and carbon-containing gases like silane and methane.[14,29,30] These approaches generated complex mixtures of reactive organosilicon species, which complicate the recognition of distinct reaction mechanisms of formation of the simple silicon–carbon clusters in the gas phase.[12,13] Yet, an elucidation of these formation pathways is imperative for an intimate understanding of the largely elusive coupling of the silicon and carbon chemistries of the interstellar

medium at the molecular level, eventually constraining the pathways to bare silicon–carbon molecules in our galaxy.

Herein, we provide compelling evidence on the directed gas-phase synthesis of the bicyclic silicon tricarbide molecule (c-SiC$_3$, **7**) along with its linear isomer (l-SiC$_3$, **9**) in the gas phase under single-collision conditions from two acyclic reactants, tricarbon (C$_3$, X$^1\Sigma_g^-$) and the silylidyne radical (SiH, X$^2\Pi$), by exploiting crossed molecular beam experiments coupled with electronic structure calculations and quasi-classical trajectory (QCT) simulations. The overall barrierless and exoergic nature of this bimolecular reaction provides an unconventional entry point to the synthesis of **7** and **9** even at ultralow temperatures in cold molecular clouds such as G+0.693–0.0027 in the Galactic Center, where the cyclic silicon dicarbide molecule (**3**) was observed[31] and also affords a mechanistic framework rationalizing the astronomical detection of **7** and **9** in the circumstellar envelope of IRC+10216.[32,33] Indeed, formation mechanisms of **7** have only been previously explored from the degradation of SiC$_3$H$_2$ isomers *via* Lyman-α photodissociation in the outer envelopes of carbon AGB stars,[34] thus, our study reveals the first account of the bottom-up synthesis of **7** *via* bimolecular reactions in circumstellar envelopes. This represents a fundamental shift in knowledge toward neutral–neutral molecular mass growth processes to silicon carbides, questioning prior viewpoints that silicon carbides can only be formed *via* photochemical degradation of higher molecular weight silicon- and carbon-containing molecules or at elevated temperatures *via* ion–molecule reactions.[35] The close agreement between experimental chemical dynamics studies and the conclusions from QCT simulations in particular reveals that molecular beam studies merged with dynamics simulations have progressed to such a sophisticated degree that polyatomic reactions involving elements from the third row of the periodic table of the elements can be untangled at the molecular level. This framework thus offers a unified, predictive picture and rare glimpse of the gas-phase chemistry and chemical bonding of isovalent systems involving silicon under single-collision conditions.

Results and discussion

Time-of-flight mass spectra

The gas-phase reaction of electronically ground state tricarbon (C_3, $X^1\Sigma_g^+$) with the silylidyne radical (SiH, $X^2\Pi$) was explored experimentally under single-collision conditions in a crossed molecular beam machine by intersecting supersonic beams of tricarbon and silylidyne radicals perpendicularly at a collision energy of 47.9 ± 0.9 kJ mol^{-1}. The helium-seeded tricarbon beam was generated *via* laser ablation of graphite (266 nm, 5 mJ pulse^{-1}),[36] while silylidyne radicals (SiH, $X^2\Pi$) were produced *via* photodissociation of helium-seeded disilane (Si_2H_6) at a fraction of 0.5%[37] (SI). Neutral reaction products were ionized through electron impact ionization with 80 eV electrons within a triply-differentially-pumped quadrupole mass spectrometer (QMS) operated at pressures of a few 10^{-12} Torr and then mass analyzed. Time-of-flight (TOF) spectra at distinct mass-to-charge ratios (m/z) were probed with reactive scattering signal observed at $m/z = 64$ ($^{28}Si^{12}C_3^+$). Accounting for the tricarbon and silylidyne reactant masses of 36 amu and 29 amu, respectively, the detection at $m/z = 64$ can be attributed to the formation of SiC_3 (64 amu) product(s) along with atomic hydrogen (1 amu) (reaction (1)). No signal was observed at $m/z = 65$ ($^{28}Si^{12}C_3H^+$, $^{29}Si^{12}C_3^+$, $^{28}Si^{13}C^{12}C_2^+$) and 66 ($^{28}Si^{12}C_3H_2^+$,

$^{29}Si^{12}C_3H^+$, $^{28}Si^{13}C^{12}C_2H^+$, $^{30}Si^{12}C_3^+$) revealing that any silyl radicals (SiH_3) or silylene (SiH_2)—if generated during the photolysis of disilane—do not react with tricarbon. The TOF spectra were then collected at $m/z = 64$ in 5° steps with respect to the center-of-mass (CM) angle (θ_{CM}) (Fig. 3b) and integrated to obtain the laboratory angular distribution (LAD) (Fig. 3a). The TOF spectra are fairly narrow and range only from about 400 to 600 μs, which is also reflected in a narrow LAD range of only 30°. This distribution is nearly symmetric with respect to the θ_{CM} and hence indicative of indirect scattering dynamics involving SiC$_3$H reaction intermediate(s) undergoing unimolecular decomposition to SiC$_3$ product(s) plus atomic hydrogen (reaction (1)).

$$C_3 \text{ (36 amu)} + SiH \text{ (29 amu)} \rightarrow SiC_3 \text{ (64 amu)} + H \text{ (1 amu) (1)}$$
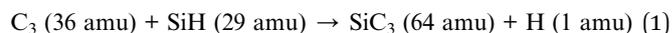
Center-of-mass flux distributions

With the detection of SiC_3 isomer(s) as a consequence of reactive single collisions between tricarbon and the silylidyne radical *via* Reaction (1), information on the chemical reaction dynamics can be obtained by converting the laboratory data into the CM reference frame.[38] This procedure yields the CM translational energy ($P(E_T)$) and angular ($T(\theta)$) flux distributions along with the associated flux contour map (Fig. 4). The laboratory data could be replicated by a single reaction channel *via* reaction (1). In detail, the best-fit $P(E_T)$ exhibits a maximum translational energy (E_{max}) of 173 ± 34 kJ mol^{-1} (Fig. 4a). For those molecules born without internal energy, the reaction energy ($\Delta_r G$) is determined to be -125 ± 35 kJ mol^{-1} by utilizing energy conservation with $\Delta_r G = E_C - E_{max}$, where E_C is the collision energy (47.9 ± 0.9 kJ mol^{-1}).[39] Additionally, the $P(E_T)$ features a distribution maximum near zero, which is indicative of a low or no barrier in the exit channel with only a slight electron density rearrangement from the fragmenting SiC$_3$H complex to the final products.[40] Further, the $T(\theta)$ (Fig. 4b) is forward–backward symmetric and exhibits intensity over the complete angular range, suggestive of indirect reactive scattering dynamics through complex formation (SiC$_3$H); this finding reinforces the conclusions drawn from the nearly symmetric LAD. The higher intensity at the poles (0° and 180°) and the dip at 90° indicates coplanar scattering dynamics, which involves geometric constraints and an emission of the hydrogen atom preferentially perpendicular to the total angular momentum vector within the rotational plane of the fragmenting complex(es).[39] These findings are also reflected in the flux contour map (Fig. 4c).

Potential energy surface

To garner insight into the underlying reaction mechanism(s) involved in the tricarbon–silylidyne system and the gas-phase preparation of SiC_3 isomer(s), the experimental results were combined with electronic structure calculations performed at the CCSD(T)-F12/aug-cc-pV(Q+d)Z//TPSSh/cc-pV(T+d)Z + ZPE (TPSSh/cc-pV(T+d)Z) level of theory.[41–44] These computations provide zero-point energy (ZPE) corrected energies of the reactants,
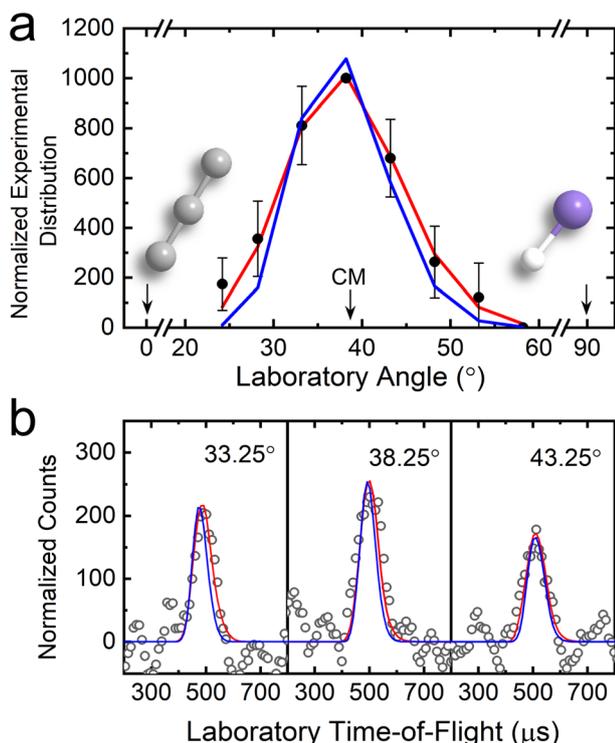

Fig. 3 Laboratory angular distribution (a) and time-of-flight spectra (b) recorded at mass-to-charge (m/z) = 64 for the reaction of tricarbon (C_3) with the silylidyne radical (SiH). CM represents the center-of-mass angle, and 0° and 90° define the directions of the tricarbon and silylidyne beams, respectively. The circles depict the experimental data, red lines the forward-convolution fits, and blue lines the MLMD simulations fits.
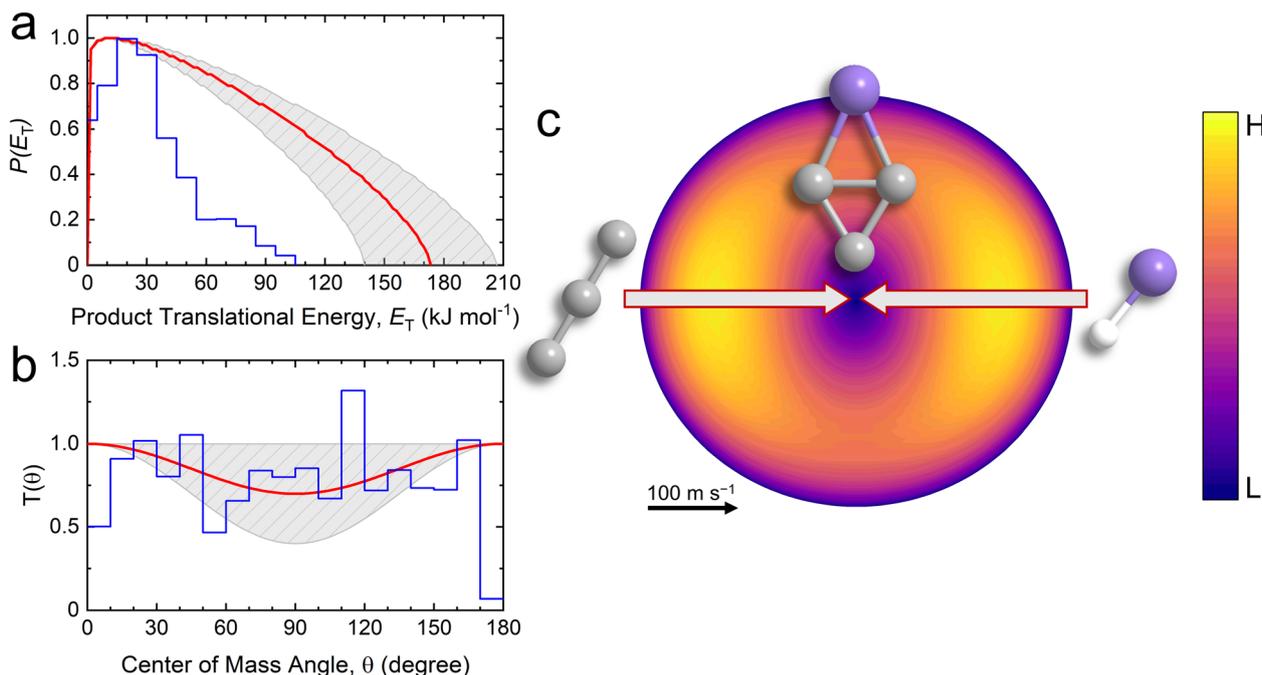
Fig. 4 Center-of-mass product translational energy (a) and angular (b) flux distributions as well as the associated flux contour map (c) leading to the formation of SiC$_3$ isomer(s) in the reaction of tricarbon (C$_3$) with the silylidyne radical (SiH). Red lines define the best-fit functions while shaded areas provide the error limits. The CM functions overlaid in blue are obtained from the MLMD simulations. The flux contour map represents the intensity of the reactively scattered products as a function of product velocity (u) and scattering angle (θ), and the color bar indicates flux gradient from low (L) to high (H) intensity.

transition states, and products with an expected accuracy of ± 5 kJ mol^{-1} (SI). The doublet SiC$_3$H potential energy surface (PES) is compiled in Fig. 5 and comprises ten SiC$_3$H reaction intermediates (**i1–i10**) and five SiC$_3$ product isomers (**p1–p5**), four of which (**p1–p4**) are formed in overall exoergic reactions releasing 109, 84, 39, and 22 kJ mol^{-1}, respectively. The experimentally observed reaction exoergicity of 125 ± 35 kJ mol^{-1} correlates well with the formation of the thermodynamically most stable carbon–carbon bisected bicyclic isomer c-SiC$_3$ (**p1**, X^{1}A$_1$, $\Delta_r G = -109 \pm 5$ kJ mol^{-1}). The energetics of the remaining exoergic hydrogen-atom-loss isomers—silicon–carbon bisected c-SiC$_3$ (**p2**, X^{1}A$_1$, $\Delta_r G = -84 \pm 5$ kJ mol^{-1}) and linear SiC$_3$ (**p3**, X$^3\Sigma^-$, $\Delta_r G = -39 \pm 5$ kJ mol^{-1})—lie outside the experimental error bars. Therefore, at least **p1** is formed. However, this does not exclude the generation of the C_{2v} symmetric **p2** and the linear **p3** isomers, since their kinetic energy release could be hidden in the lower energy section of the $P(E_T)$.

How can the bicyclic product **p1** be synthesized as the result of a single collision of two acyclic reactants? The electronic structure calculations identified two barrierless entrance channels *via* addition of the silylidyne radical (SiH, X$^2\Pi$) either to one terminal carbon atom of tricarbon (C$_3$, X$^1\Sigma_g^+$) or to both terminal carbon atoms simultaneously yielding the acyclic and bicyclic doublet intermediates **i1** and **i2**, respectively. The barrierless nature of these entrance channels was verified by optimized PES scans following the reaction coordinate. From these initial collision complexes, there are a plethora of possible pathways to **p1**. Both intermediates can be interconverted easily *via* a transition state ranging

212 kJ mol^{-1} below the energy of the separated reactants. This isomerization involves the simultaneous formation of two silicon–carbon bonds of 196 pm and 231 pm lengths producing a bicyclic structure (**i1 → i2**). These bonds are slightly elongated compared to the carbon–silicon single bond in methylsilane (CH$_3$SiH$_3$)[45] and hence can be classified as sigma bonds. The central silicon–carbon bond in **i2** then breaks, and a new bond forms between the outer two carbon atoms generating a diamond-like intermediate (**i2 → i3**) followed by barrierless hydrogen atom loss to **p1**. Alternatively, **i1** can isomerize in one step to **i3** *via* a synchronous formation of a carbon–carbon and carbon–silicon bond (**i1 → i3**). Both intermediates **i4** and **i8** may also decompose *via* hydrogen atom loss to **p1**, with the most energetically-favorable routes involving a hydrogen migration and ring closure from **i1** to **i5** followed by C–Si bisecting bond breaking and C–C bisecting bond reforming from **i5** to **i4** (**i1 → i5 → i4 → p1**), and [1,2]-hydrogen shift from **i4** to **i8** (**i1 → i5 → i4 → i8 → p1**). The unimolecular decomposition of **i3**, **i4**, and **i8** are all barrierless (loose exit transition states) as verified experimentally in the close-to-zero peaking of the center-of-mass translational energy distribution.

The second bicyclic SiC$_3$ isomer **p2** as well as the linear structure **p3** may also have been synthesized *via* the bimolecular reaction of tricarbon with the silylidyne radical. First, **p2** can be accessed *via* unimolecular decomposition of intermediates **i2** and/or **i5** accompanied by atomic hydrogen loss; the energetically most likely pathways involve first a ring closure from **i1** to the bicyclic backbone moiety (**i1 → i2 → p2; i1 → i5 → p2**) and/or a simple addition–elimination from **i2** followed by hydrogen
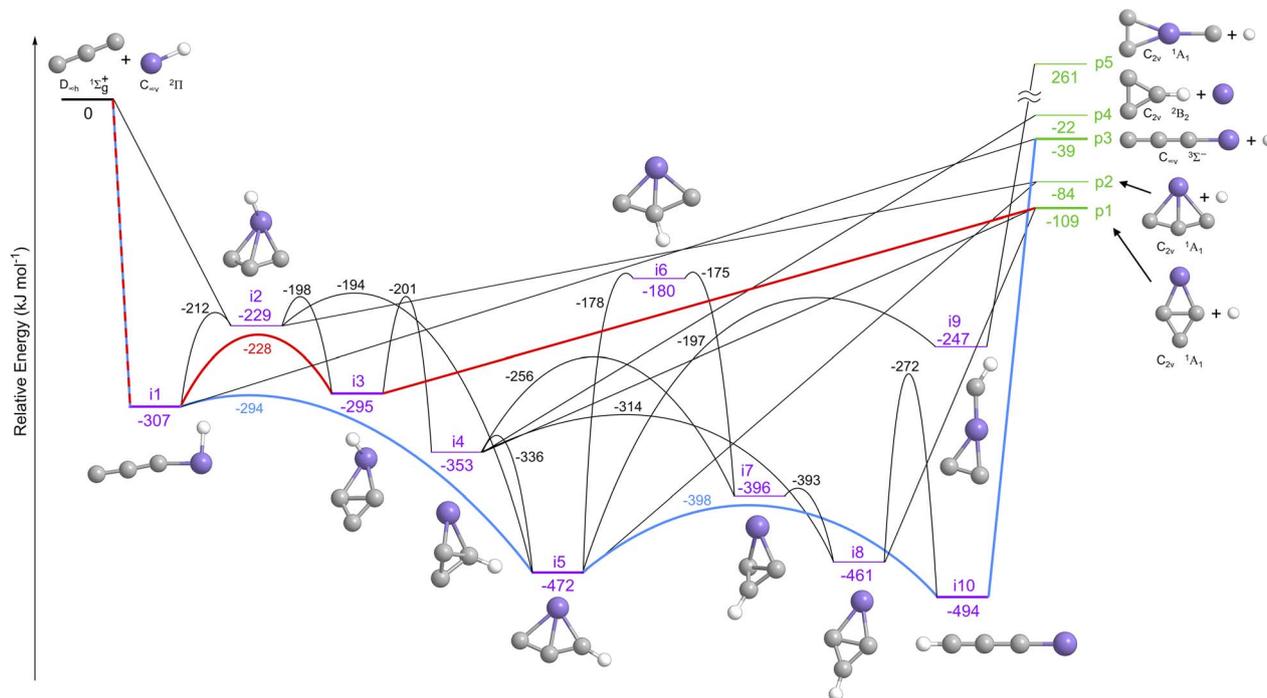
Fig. 5 Schematic potential energy surface (PES) for the reaction of tricarbon (C_3) with the silylidyne radical (SiH) leading to the four most stable SiC_3 isomers calculated at the CCSD(T)-F12/aug-cc-pV(Q+d)Z//TPSSh/cc-pV(T+d)Z + ZPE(TPSSh/cc-pV(T+d)Z) level. Relative energies are given in kJ mol^{-1}, and point groups and electronic states are provided for reactants and products. Energy levels of intermediates are shown in purple and those of products are shown in green. The most probable reaction pathways to the astronomically observed species **p1** and **p3** are highlighted in red and blue, respectively.

atom loss (**i2** → **p2**). Second, **p3** may be prepared *via* atomic hydrogen loss from intermediates **i1** and/or **i10** *via* a simple addition–elimination process (**i1** → **p3**) or through the energetically most favorable cyclization–ring-opening route passing through **i10** (**i1** → **i5** → **i10** → **p3**). Overall, the computational results support the experimental detection of at least the thermodynamically most stable bicyclic isomer (**p1**) accessed *via* a barrierless, bimolecular, exoergic reaction of electronically ground state tricarbon (C_3, $X^1\Sigma_g^+$) with the silylidyne radical (SiH, $X^2\Pi$), while both **p2** and **p3** also feature possible routes under our experimental conditions.

Quasi-classical trajectory simulations

To identify the most likely reaction pathways and illustrate how the reaction progresses, reaction dynamics simulations were performed. 3600 bimolecular collision machine-learned molecular dynamics (MLMD) trajectories were simulated for 15 ps or until dissociation to reactants or products. Of these, 2068 trajectories formed intermediates or products, resulting in product branching ratios of 63% **p1**, 22% **p2**, 2% **p3**, and 13% **p4**, with no formation of the high-energy product **p5**. For the reaction pathways, the trajectories show no direct product formation, *i.e.*, all are indirect with finite lifetimes of intermediates before dissociating. Due to the large potential energy release from the bimolecular association, isomerization between intermediates is extremely fast, with more than one million recorded over all trajectories. To quantify precise

statistical probabilities of these events, the reaction mechanism can be formulated as a Markov process, where a sequence of transitions between discrete states takes place. The states are defined as critical points on the PES, thus the transitions correspond to isomerization processes. The probability of product formation from each unimolecular state is shown in Fig. 6, where exit channels to **p1**, **p2**, and **p3** mostly originate from **i3**, **i5**, and **i10**, respectively. From the MLMD simulations and Markov model, the most probable reaction pathway involves the entrance channel to **i1**, followed by cyclization to **i3** and atomic hydrogen loss forming the experimentally observed bicyclic silicon tricarbide molecule (**p1**). More details regarding the QCT simulations are given in the SI accompanied by Fig. S1–S9 and Tables S1–S6.

Finally, the dynamics were validated against experimental results. Although the experiments do not have information on the time evolution of the intermediates, they contain information on the products such as scattering angles and translational energies. To match the experimental detection, only hydrogen-atom-loss products (**p1**, **p2**, and **p3**) were tallied. As shown in Fig. 4, the scattering angle distributions of the experimental fit and the MLMD agree qualitatively. While the translational energy distributions disagree on maximum energies, they have similar most-probable energies. In general, products with high translational energy are rare and difficult to measure in MD simulations, often leading to mismatches between experimental and MD distributions at
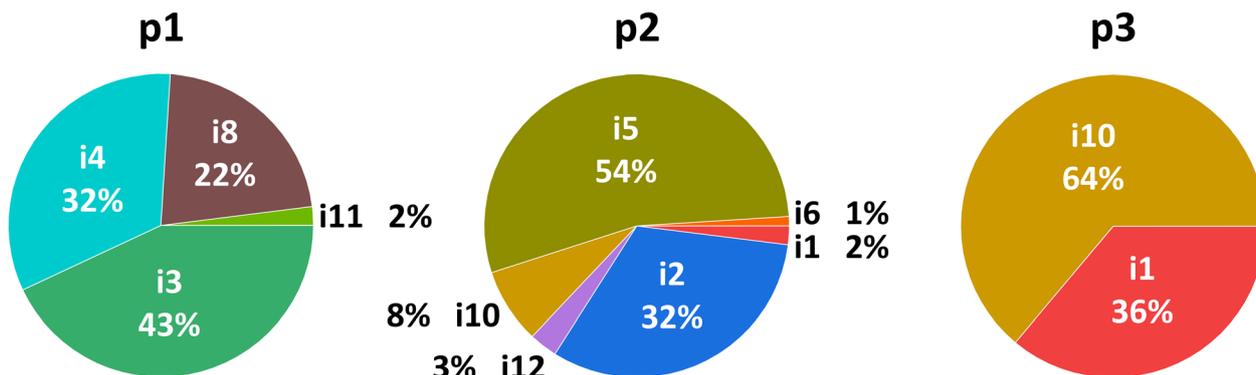
Fig. 6 Transition probabilities from different intermediates to products **p1**, **p2**, and **p3**, represented as percentages, shown as pie charts.

the high-energy tail, as reported in similar studies.[46–48] Extending the MLMD simulations is not likely to resolve this issue, as the longer the lifetime of an intermediate, the more inelastic the collision becomes, and the less translational energy the products retain. A more solid comparison between the MLMD simulations and the experiment can come by
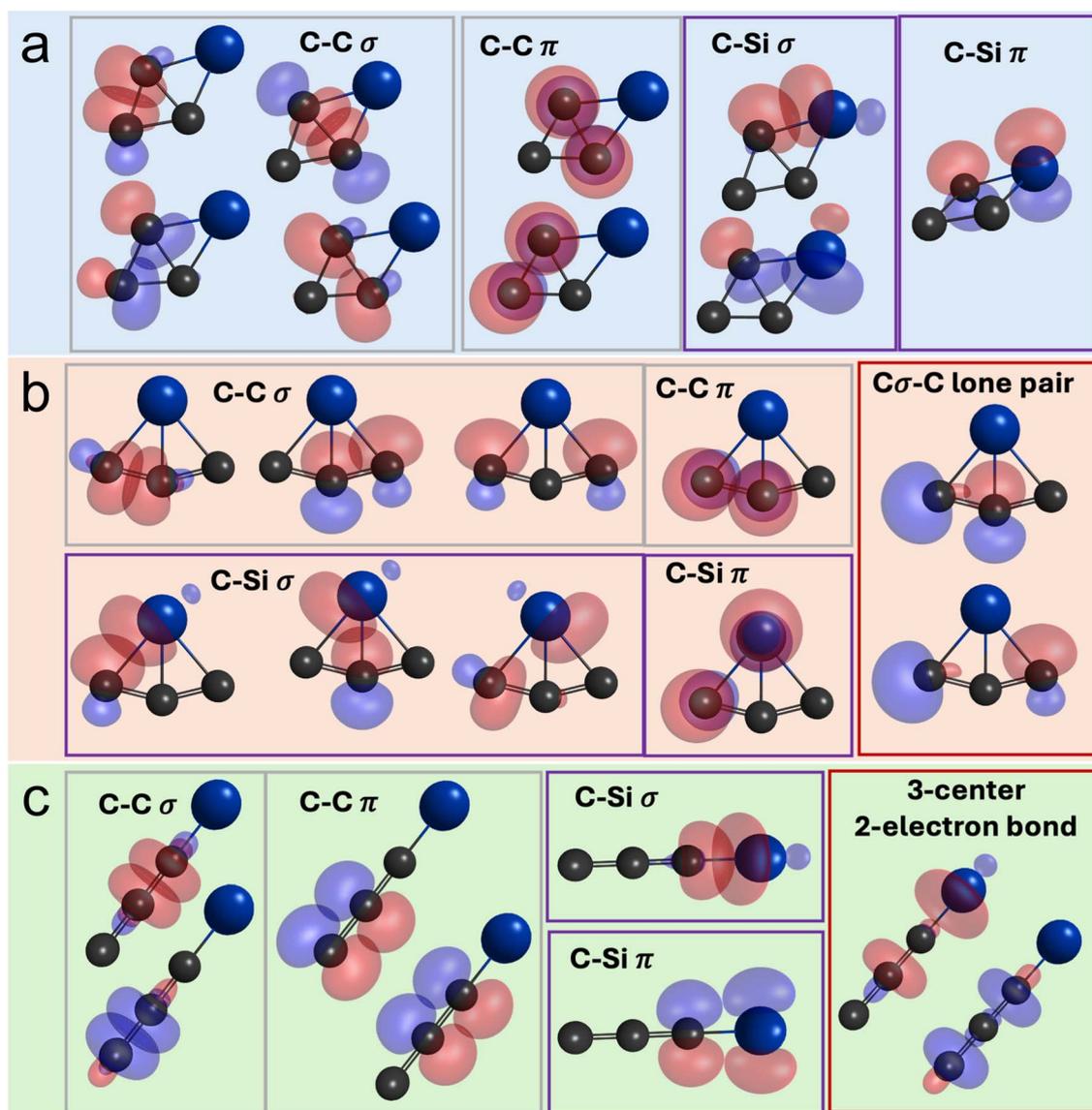

Fig. 7 Quasi-atomic orbital analysis (QUAO) of distinct SiC_3 isomers **p1** (a), **p2** (b), and **p3** (c).

directly forward-convoluting the MLMD simulations' CM distributions to the raw lab data as shown in Fig. 3, where the data agree well.

Quasi-atomic orbital analysis

As the hydrogen atom is ejected during the transformation from **i3** to **p1**, multiple structural changes occur within the SiC_3 moiety. The carbon–carbon bisecting bond shrinks from 152 to 148 pm while the peripheral carbon–carbon bonds elongate from 135 to 144 pm. In addition, the silicon–carbon bonds are reduced from 197 to 184 pm essentially shifting the bisected bond towards the silicon atom. This results in an increased C–Si–C angle of 47.4° and reduced opposing C–C–C angle of 62.0°. The structural changes could reflect inclusion of the silicon atom within the π electron delocalized system and shift to 2π aromaticity. As for the linear SiC_3 isomer, the conversion from **i10** to **p3** invokes a silicon–carbon bond elongation from 170 to 173 pm, C_1–C_2 carbon–carbon bond shortening from 133 to 129 pm, and a lengthening of the C_2–C_3 carbon–carbon bond from 123 to 131 pm. These changes likely indicate a shift from a butadiyne-type structure to cumulenic bonding as the hydrogen atom is ejected. Fundamental insights into the chemical bonding of these SiC_3 isomers can be further obtained from quasi-atomic orbital (QUAO) analysis (Fig. 7) highlighting the orbitals that participate in (covalent) bonding interactions.[49–54] In this analysis, the kinetic bond order (KBO) represents a measure of the strength of the bonding interaction, while the occupation numbers in two orbitals are the number of electron populations involved in the covalent bond (Table S7). Generally, for all isomers, the strengths of the carbon–silicon σ and π bonds (KBOs = −105 to −63 and −42 to −8 kJ mol^{-1}, respectively) significantly decreases compared to the isovalent carbon–carbon bond interactions (KBOs = −293 to −167 and −71 to −33 kJ mol^{-1} for σ and π bonds, respectively). In all isomers, the interference kinetic energy, *i.e.* the fundamental origin of the covalent bond,[55–59] is mainly the result of the σ bonding interactions (64–84%), while the π bonds contribute 15–34%. From the QUAO analysis, the stability of the bicyclic SiC_3 isomer **p1** is based on the strong carbon–silicon σ interactions with contributions of 23, 17, and 11% for isomers **p1**, **p2**, and **p3**, respectively, while minor contributions of 4, 2, and 8% arise from π interactions. In bicyclic **p1** and **p2**, an additional stabilization arises from the lateral overlap between the C–C and Si–C σ interactions. Such an orbital overlap of silicon with the peripheral carbon in **p2** is in excellent agreement with the previous theoretical study by Rintelman and Gordon.[15] Interestingly, **p3** exhibits interactions between three center atoms with electron populations of 1.7 to 2.0, which is indicative of a three-center-two-electron interaction type (Fig. S10 and Table S7).

Conclusions

The crossed molecular beam experiments in conjunction with electronic structure calculations and QCT simulations provide a unique glimpse into the distinct dynamics of isovalent systems at the fundamental, microscopic level benchmarked

with the gas-phase synthesis of silicon tricarbide molecules in their carbon–carbon (c-SiC_3, X^1A_1, **p1**) and silicon–carbon (c-SiC_3, X^1A_1, **p2**) bisected bicyclic forms along with the linear isomer (l-SiC_3, $X^3\Sigma^-$, **p3**) from the bimolecular reaction of the acyclic tricarbon (C_3, $X^1\Sigma_g^+$) and silylidyne radical (SiH, $X^2\Pi$) reactants. The addition of the silicon atom of the silylidyne radical to a terminal carbon atom of tricarbon proceeds without barrier, followed by exotic ring-formation through doublet silabicyclobutadienyl intermediates (c-SiC_3H) either forming **p1** or **p2** coupled with atomic hydrogen loss, or isomerizing through ring-opening to a 2-propynylidynesilyl structure (l-HC_3Si) followed by hydrogen atom loss to **p3**. While the two most stable structures of silicon tricarbide are bicyclic with 34 and 9 kJ mol^{-1} lower energy than the linear structure, the ground state of the isovalent tetracarbon molecule is not bicyclic; the linear structure (C_4, $X^3\Sigma_g^-$) is more stable by 9 kJ mol^{-1} (Fig. 2b). This demonstrates the dramatic effects substituting just one carbon atom with an isovalent silicon atom has on chemical structure and electronic properties. The inherent QUAO analysis and interference kinetic energies of the three SiC_3 isomers offer evidence of primary bonding interactions originating from the σ bonding motifs: while carbon–carbon σ bonds contribute about 60% of the interference kinetic energy, the percent contributions of the carbon–silicon σ bonds in bicyclic SiC_3 isomers **p1** and **p2** of 23 and 17%, respectively, are significantly larger than those in the linear isomer **p3** (11%).

Silicon–carbon bond coupling and the formation of silicon carbide clusters signifies a crucial topic not only for fundamental reaction dynamics and chemical bonding, but also for the astronomy and astrochemistry communities. Recently, dust particles produced from modeling the condensation of silicon carbide (SiC) and 1,3,5-trisiladehydrobenzene (Si_3C_3) clusters in asymptotic giant branch (AGB) stellar winds of carbon rich stars showed a match with common SiC emission lines observed astronomically.[60] These spectral similarities extend to small- and mid-size clusters ranging up to $Si_{16}C_{16}$,[61] further reinforcing the importance of exploring the fundamental formation mechanisms of silicon carbides under astrophysically relevant conditions.

With the tricarbon molecule detected in the circumstellar envelope of the carbon star IRC+10216 (ref. 62) and predicted to exist in cold molecular clouds[63] and the silylidyne radical generated *via* photodissociation and galactic comic ray degradation of silane (SiH_4), the title reaction provides a unique entry point into an exotic silicon–carbon chemistry and molecular mass growth processes involving silicon in deep space as evidenced by the formation of the astronomically observed silicon tricarbide molecules **p1** and **p3**. The elucidated bottom-up mechanisms are of fundamental significance to facilitate an understanding of how carbon and silicon chemistries can be coupled and hence challenge conventional wisdom that silicon carbides can only be formed at elevated temperatures *via* complex ion–molecule reactions or degradation of higher molecular weight silicon carbon molecules.[35] This system exemplifies the versatile concept of barrierless and exoergic molecular mass growth processes to silicon carbides from acyclic precursors potentially adaptable to the multifaceted reaction sequence Reaction (2). With the full-scale operation of the Atacama Large

Millimeter/Submillimeter Array, the detection of unusual silicon-bearing molecules is expected to increase significantly. Interpreting these observations will depend critically on advances in experimental and computational laboratory astrophysics, as proposed in this work. Such progress is essential to bridge the longstanding gap between observational data and laboratory studies of organosilicon chemistry in the galaxy.

$$C_n + SiH \rightarrow SiC_n + H \tag{2}$$

Author contributions

S. J. G. and R. I. K. conceptualized the experiments; S. J. G., Z. Y., S. M., and I. A. M. conducted the experiments; R. I. K. supervised the experiments; M. O. A. and M. X. S. performed the electronic structure calculations; B. R. L. G. supervised the electronic structure calculations; K. F. performed the quasi-classical trajectory simulations; R. S. supervised the quasi-classical trajectory simulations; T. S. performed the quasi-atomic orbital analysis; S. J. G. and K. F. wrote the original draft of the manuscript; S. J. G., K. F., R. I. K., B. R. L. G., R. S., and T. S. revised the draft of the manuscript with input from all authors.

Conflicts of interest

There are no conflicts to declare.

Data availability

The data that support the findings of this study are available in the article and the supplementary information (SI). Additional data are available from the corresponding authors upon request. Supplementary information: experimental methods, computational methods, details of AIMD simulations, comparison of different MD methods (Table S1), benchmarking the sGDML potential, energy and force errors (Fig. S1), training set representation (Fig. S2), reaction probability method comparison (Fig. S3), complete MLMD results, reaction probability for different products (Fig. S4), transition probabilities (Table S2), product transition probabilities (Fig. S5), details of the Markov model, Markov digraph (Fig. S6), DFT PES (Fig. S7), product branching ratios (Table S3), chemical concentration curves (Fig. S8), intermediate lifetime distributions (Fig. S9), intermediate lifetime fits (Table S4 and S5), semi-Markov stationary states (Table S6), QUAO analysis of SiC3 isomers, presentation of QUAOs (Fig. S10), QUAO analysis values (Table S7), Cartesian coordinates and vibrational frequencies for all species (Data S1), supplementary references. See DOI: https://doi.org/10.1039/d6sc00002a.

Acknowledgements

Notes and references

1 P. Thaddeus, S. E. Cummins and R. A. Linke, *Astrophys. J.*, 1984, **283**, L45–L48.

2 R. Papoular, M. Cauchetier, S. Begin and G. LeCaer, *Astron. Astrophys.*, 1998, **329**, 1035–1044.

3 H. Fueno and Y. Taniguchi, *Chem. Phys. Lett.*, 1999, **312**, 65–70.

4 H. S. P. Müller and D. E. Woon, *J. Phys. Chem. A*, 2013, **117**, 13868–13877.

5 A. J. C. Varandas and C. M. R. Rocha, *Philos. Trans. R. Soc., A*, 2018, **376**, 1–46.

6 G. Maier, H. Pacl, H. P. Reisenauer, A. Meudt and R. Janoschek, *J. Am. Chem. Soc.*, 1995, **117**, 12712–12720.

7 T. J. Butenhoff and E. A. Rohlfing, *J. Chem. Phys.*, 1991, **95**, 1–8.

8 E. Clementi, H. Kistenmacher and H. Popkie, *J. Chem. Phys.*, 1973, **58**, 2460–2466.

9 S. C. Ross, T. J. Butenhoff, E. A. Rohlfing and C. M. Rohlfing, *J. Chem. Phys.*, 1994, **100**, 4110–4126.

10 I. M. B. Nielsen, W. D. Allen, A. G. Császár and H. F. Schaefer, III, *J. Chem. Phys.*, 1997, **107**, 1195–1211.

11 C. M. R. Rocha, H. Linnartz and A. J. C. Varandas, *J. Chem. Phys.*, 2022, **157**, 104301.

12 M. C. McCarthy, A. J. Apponi and P. Thaddeus, *J. Chem. Phys.*, 1999, **110**, 10645–10648.

13 A. J. Apponi, M. C. McCarthy, C. A. Gottlieb and P. Thaddeus, *J. Chem. Phys.*, 1999, **111**, 3911–3918.

14 M. C. McCarthy, A. J. Apponi, C. A. Gottlieb and P. Thaddeus, *Astrophys. J.*, 2000, **538**, 766–772.

15 J. M. Rintelman and M. S. Gordon, *J. Chem. Phys.*, 2001, **115**, 1795–1803.

16 I. Langmuir, *J. Am. Chem. Soc.*, 1919, **41**, 868–934.

17 N. Job and K. Thirumoorthy, *ACS Earth Space Chem.*, 2024, **8**, 467–482.

18 J. Bernal, P. Haenecour, J. Howe, T. Zega, S. Amari and L. Ziurys, *Astrophys. J., Lett.*, 2019, **883**, L43.

19 T. Chen, C. Y. Xiao, A. Li and C. T. Zhou, *Mon. Not. R. Astron. Soc.*, 2021, **509**, 5231–5236.

20 P. R. Heck, J. Greer, L. Kööp, R. Trappitsch, F. Gyngard, H. Busemann, C. Maden, J. N. Ávila, A. M. Davis and R. Wieler, *Proc. Natl. Acad. Sci. U. S. A.*, 2020, **117**, 1884–1889.

21 S. R. Kulkarni, V. K. Velisoju, F. Tavares, A. Dikhtiarenko, J. Gascon and P. Castaño, *Catal. Rev.*, 2023, **65**, 174–237.

22 O. Arayawut, T. Kerdcharoen and C. Wongchoosuk, *Nanomaterials*, 2022, **12**, 1869.

23 F. Ullah, N. Kosar, M. N. Arshad, M. A. Gilani, K. Ayub and T. Mahmood, *Opt. Laser Technol.*, 2020, **122**, 105855.

24 P. Miró, M. Audiffred and T. Heine, *Chem. Soc. Rev.*, 2014, **43**, 6537–6554.

25 R. Suenram, F. Lovas and K. Matsumura, *Astrophys. J., Lett.*, 1989, **342**, L103–L105.

26 M. A. Capano, *J. Appl. Phys.*, 1995, **78**, 4790–4792.

27 S. H. Nam and S. M. Park, *Appl. Phys. A*, 2004, **79**, 1117–1120.

28 D. Witsch, V. Lutter, A. A. Breier, K. M. T. Yamada, G. W. Fuchs, J. Gauss and T. F. Giesen, *J. Phys. Chem. A*, 2019, **123**, 4168–4177.

29 B. Gans, J. Liévin, P. Halvick, N. L. Chen, S. Boyé-Péronne, S. Hartweg, G. A. Garcia and J. C. Loison, *Phys. Chem. Chem. Phys.*, 2023, **25**, 23568–23578.

30 M. C. McCarthy, J. H. Baraban, P. B. Changala, J. F. Stanton, M.-A. Martin-Drumel, S. Thorwirth, C. A. Gottlieb and N. J. Reilly, *J. Phys. Chem. Lett.*, 2015, **6**, 2107–2111.

31 S. Massalkhi, I. Jiménez-Serra, J. Martín-Pintado, V. M. Rivilla, L. Colzi, S. Zeng, S. Martín, B. Tercero, P. de Vicente and M. A. Requena-Torres, *Astron. Astrophys.*, 2023, **678**, A45.

32 A. J. Apponi, M. C. McCarthy, C. A. Gottlieb and P. Thaddeus, *Astrophys. J.*, 1999, **516**, L103–L106.

33 J. Cernicharo, J. R. Pardo, M. Agúndez, J. P. Fonfría, L. Velilla-Prieto, C. Cabezas, B. Tercero, P. de Vicente and M. Guélin, *Astron. Astrophys.*, 2025, **700**, L20.

34 T. Yang, L. Bertels, B. B. Dangi, X. Li, M. Head-Gordon and R. I. Kaiser, *Proc. Natl. Acad. Sci. U. S. A.*, 2019, **116**, 14471–14478.

35 A. Glassgold and G. Mamon, in *Chemistry and Spectroscopy of Interstellar Molecules*, ed. D. Bohme, University of Tokyo Press, Tokyo, 1992, p. 261.

36 R. I. Kaiser, T. N. Le, T. L. Nguyen, A. M. Mebel, N. Balucani, Y. T. Lee, F. Stahl, P. v. R. Schleyer and H. F. Schaefer III, *Faraday Discuss.*, 2002, **119**, 51–66.

37 T. Yang, B. B. Dangi, A. M. Thomas and R. I. Kaiser, *Chem. Phys. Lett.*, 2016, **654**, 58–62.

38 R. I. Kaiser, C. Ochsenfeld, D. Stranges, M. Head-Gordon and Y. T. Lee, *Faraday Discuss.*, 1998, **109**, 183–204.

39 W. B. Miller, S. A. Safron and D. R. Herschbach, *Discuss. Faraday Soc.*, 1967, **44**, 108–122.

40 J. Laskin and C. Lifshitz, *J. Mass Spectrom.*, 2001, **36**, 459–478.

41 H. J. Werner, P. J. Knowles, G. Knizia, F. R. Manby, M. Schütz, P. Celani, W. Györffy, D. Kats, T. Korona, R. Lindh, A. Mitrushenkov, G. Rauhut, K. R. Shamasundar, T. B. Adler, R. D. Amos, A. Bernhardsson, A. Berning, D. L. Cooper, J. O. Deegan, A. J. Dobbyn, F. Eckert, E. Goll, C. Hampel, A. Hesselmann, G. Hetzer, T. Hrenar, G. Jansen, C. Köppl, Y. Liu, A. W. Lloyd, R. A. Mata, A. J. May, S. J. McNicholas, W. Meyer, M. E. Mura, A. Nicklass, D. P. O'Neill, P. Palmieri, D. Peng, K. Pflüger, R. Pitzer, M. Reiher, T. Shiozaki, H. Stoll, A. J. Stone, R. Tarroni, T. Thorsteinsson and M. Wang, *MOLPRO, a package of ab initio programs, Version 2015.1*, University of Cardiff, Cardiff, UK, 2015.

42 T. H. Dunning Jr, K. A. Peterson and A. K. Wilson, *J. Chem. Phys.*, 2001, **114**, 9244–9253.

43 T. B. Adler, G. Knizia and H.-J. Werner, *J. Chem. Phys.*, 2007, **127**, 221106.

44 G. Knizia, T. B. Adler and H.-J. Werner, *J. Chem. Phys.*, 2009, **130**, 054104.

45 R. W. Kilb and L. Pierce, *J. Chem. Phys.*, 1957, **27**, 108–112.

46 C. He, K. Fujioka, A. A. Nikolayev, L. Zhao, S. Doddipatla, V. N. Azyazov, A. M. Mebel, R. Sun and R. I. Kaiser, *Phys. Chem. Chem. Phys.*, 2022, **24**, 578–593.

47 S. J. Goettl, A. Vincent, M. X. Silva, Z. Yang, B. R. L. Galvão, R. Sun and R. I. Kaiser, *Sci. Adv.*, 2024, **10**, eadq5018.

48 S. Doddipatla, C. He, R. I. Kaiser, Y. Luo, R. Sun, G. R. Galimova, A. M. Mebel and T. J. Millar, *Proc. Natl. Acad. Sci. U. S. A.*, 2020, **117**, 22712–22719.

49 A. C. West, M. W. Schmidt, M. S. Gordon and K. Ruedenberg, *J. Chem. Phys.*, 2013, **139**, 234107.

50 A. C. West, M. W. Schmidt, M. S. Gordon and K. Ruedenberg, *J. Phys. Chem. A*, 2015, **119**, 10360–10367.

51 A. C. West, M. W. Schmidt, M. S. Gordon and K. Ruedenberg, *J. Phys. Chem. A*, 2017, **121**, 1086–1105.

52 K. Ruedenberg, *J. Chem. Phys.*, 2022, **157**, 024111.

53 K. Ruedenberg, *J. Chem. Phys.*, 2022, **157**, 210901.

54 D. Del Angel Cruz, K. N. Ferreras, T. Harville, G. Schoendorff and M. S. Gordon, *Phys. Chem. Chem. Phys.*, 2024, **26**, 21395–21406.

55 W. Kutzelnigg and W. H. E. Schwarz, *Phys. Rev. A*, 1982, **26**, 2361–2367.

56 G. B. Bacskay, *J. Chem. Phys.*, 2022, **156**, 204122.

57 G. Frenking, *Mol. Phys.*, 2023, **121**, e2110168.

58 L. Zhao, S. Pan, N. Holzmann, P. Schwerdtfeger and G. Frenking, *Chem. Rev.*, 2019, **119**, 8781–8845.

59 W. Kutzelnigg, *Angew. Chem., Int. Ed.*, 1973, **12**, 546–562.

60 R. Wu, C. Zhu, G. Lü, S. Yang, Z. Meng, X. Zhang, X. Lu, J. Yu, W. Chen and M. Long, *Res. Astron. Astrophys.*, 2024, **24**, 055002.

61 D. Gobrecht, S. Cristallo, L. Piersanti and S. T. Bromley, *Astrophys. J.*, 2017, **840**, 117.

62 K. W. Hinkle, J. J. Keady and P. F. Bernath, *Science*, 1988, **241**, 1319–1322.

63 A. M. Mebel, M. Agúndez, J. Cernicharo and R. I. Kaiser, *Astrophys. J., Lett.*, 2023, **945**, L40.